HKU CS Tech Report TR-2010-08

Obtuse Triangle Suppression in Anisotropic Meshes

Feng Sun[a], Yi-King Choi[a], Wenping Wang[a], Dong-Ming Yan[a,b], Yang Liu[b,c], Bruno Lévy[b]

[a] *Department of Computer Science, The University of Hong Kong, Pokfulam Road, Hong Kong, China*

[b] *LORIA/INRIA Lorraine, Project ALICE, Campus scientifique 615, rue du Jardin Botanique, 54600, Villers les Nancy, France*

[c] *Microsoft Research Asia, 5/F, Beijing Sigma Center, No.49, Zhichun Road, Haidian District, Beijing, 100190, China*

Abstract

Anisotropic triangle meshes are used for efficient approximation of surfaces and flow data in finite element analysis, and in these applications it is desirable to have as few obtuse triangles as possible to reduce the discretization error. We present a variational approach to suppressing obtuse triangles in anisotropic meshes. Specifically, we introduce a *hexagonal Minkowski metric*, which is sensitive to triangle orientation, to give a new formulation of the centroidal Voronoi tessellation (CVT) method. Furthermore, we prove several relevant properties of the CVT method with the newly introduced metric. Experiments show that our algorithm produces anisotropic meshes with much fewer obtuse triangles than using existing methods while maintaining mesh anisotropy.

Keywords: triangulation, Minkowski metric, anisotropic mesh, surface remeshing, obtuse triangles

1. Introduction

Anisotropic meshes are used to approximate surfaces or flow fields for rendering and simulation (Cohen-Steiner et al. [2004], Dey et al. [2007], Valette et al. [2008]). For anisotropic triangle meshes to be used in finite element methods (FEM), it has been well established (Babuska and Aziz [1976], Bern and Eppstein [1992a], Shewchuk [2002]) that the accuracy and convergence of the interpolation function in FEM are greatly influenced by the maximal angle of a triangle element. Triangles with large angles are also found to hamper the efficiency of some iterative algebraic solvers (Du et al. [2005]). This implies that obtuse triangles should be avoided as much as possible[1]. The control of the maximum angle is difficult, however. Existing methods for anisotropic triangulation always produce meshes that contain a large number of obtuse triangles.

Email addresses: fsun@cs.hku.hk (Feng Sun), ykchoi@cs.hku.hk (Yi-King Choi), wenping@cs.hku.hk (Wenping Wang), dmyan@cs.hku.hk (Dong-Ming Yan), liuyang@loria.fr (Yang Liu), levy@inria.fr (Bruno Lévy)

[1] In some cases where the mesh anisotropy is dictated by the anisotropy of a PDE to be solved on the mesh, obtuse triangles with certain orientations are acceptable (Shewchuk [2002]).

There are a number of methods for computing anisotropic triangulations. The algorithms in Leibon and Letscher [2000], Cheng et al. [2006], Labelle and Shewchuk [2003] compute an anisotropic Voronoi diagram of some fixed data points, whose dual is an anisotropic triangulation. To allow unconstrained vertices, a number of methods have been proposed (e.g., Bossen and Heckbert [1996], Shimada [1997], Du et al. [2005], Wang and Du [2005], Jiao et al. [2006], Boissonnat et al. [2008]). Anisotropic triangulations that minimize interpolation errors of an underlying function or surface are characterized in Simpson [1994], Rippa [1992]. Based on similar considerations, data-dependent triangulation of fixed data points are studied in Dyn et al. [1990, 2001]. However, none of these methods consider avoiding obtuse triangles.

While nonobtuse triangulation has been the topic of considerable research, little is known about how to remove or suppress obtuse triangles in anisotropic triangulations. Existing methods for computing nonobtuse triangulations (e.g., Baker et al. [1988], Bern and Eppstein [1992b], Li and Zhang [2006], Brandts et al. [2009]) are not applicable to anisotropic meshes as they do not take the anisotropy requirement into consideration. In this paper, we present an effective method for suppressing obtuse triangles in anisotropic triangle meshes while maintaining mesh anisotropy. Our contribution is the introduction of a novel *hexagonal Minkowski metric* in the formulation of the centroidal Voronoi tessellation (CVT) method, based on which a variational method is devised for computing anisotropic meshes. In addition, we also prove several properties of the CVT method with the newly introduced metric. Our method is capable of producing anisotropic triangulations that have much fewer obtuse triangles than using existing methods.

2. Preliminaries

A commonly used approach to anisotropic triangulation is based on *anisotropic centroidal Voronoi tessellation* (anisotropic CVT). In this approach, an energy function is first defined for a set of points, called *seeds*, in a compact domain Ω. This energy function is then minimized to determine the optimal distribution of the seeds. Finally, a triangle mesh is obtained by taking the seeds as mesh vertices and using the dual of the Voronoi diagram of the seeds to determine edge connectivity of the mesh. Two keys to successful application of such a CVT-based method are: 1) the formulation of an appropriate CVT energy function reflecting the desired mesh quality criteria (e.g., anisotropy, orientation control, mesh density); and 2) the development of effective optimization schemes for minimizing this function (e.g., initialization, convergence, avoidance of poor local minima).

We will briefly introduce the concepts of *anisotropic CVT*, on which our triangulation algorithm is based. We first present the basics about isotropic centroidal Voronoi tessellation (isotropic CVT) which are necessary for a good understanding of anisotropic CVT. We assume a two-dimensional compact domain Ω for the simplicity of explanation, but the concepts to be introduced apply also to the more general domains, including surfaces.

Isotropic CVT. Let $\mathbf{X} = (\mathbf{x}_i)_{i=1}^n$ be an ordered set of points, called *seeds* or *generators*, in Ω. The Voronoi cell Ω_i, also called the CVT cell, of a seed $\mathbf{x}_i$ is

$$\Omega_i = \{\mathbf{x} \in \Omega \mid d(\mathbf{x}, \mathbf{x}_i) \leq d(\mathbf{x}, \mathbf{x}_j), \forall j \neq i, j = 1, 2, \ldots, n\}$$

where $d(\mathbf{x}, \mathbf{y})$ is the Euclidean distance between the points $\mathbf{x}$ and $\mathbf{y}$. The collection of the Voronoi cells Ω_i of all the seeds $\mathbf{x}_i$ constitutes a Voronoi tessellation (or Voronoi diagram) of Ω. A *constrained centroid* of Ω_i is the point in Ω_i that is closest to the centroid (i.e., the center of mass) of Ω_i; note that the constrained centroid agrees with the centroid when the centroid is inside Ω_i. A *centroidal Voronoi tessellation*, or CVT, is a special Voronoi tessellation in which each seed $\mathbf{x}_i$ coincides with the constrained centroid $\mathbf{c}_i$ of its Voronoi cell Ω_i (Du et al. [1999]).

From a variational standpoint, a CVT is characterized by a critical point (i.e., a gradient-vanishing point) of the following isotropic CVT energy function (Du et al. [1999])

$$F(\mathbf{X}) = \sum_{i=1}^{n} F_i(\mathbf{X}) = \sum_{i=1}^{n} \int_{\Omega_i} d^2(\mathbf{x}, \mathbf{x}_i) \mathrm{d}\sigma \tag{1}$$

where $\mathrm{d}\sigma$ is the differential area element of Ω. In practice, we seek to compute a CVT corresponding to a local minimizer of $F(\mathbf{X})$ and such a CVT will be called a *stable CVT*. Furthermore, a CVT given by a global minimizer of $F(\mathbf{X})$ will be called an *optimal CVT*. The most commonly used method for minimizing the CVT energy function is the Lloyd's method (Du et al. [1999]), and a more efficient quasi-Newton method is recently proposed by Liu et al. [2009].

According to the celebrated Gersho's conjecture (Gersho [1979]), as the number of seeds increases, the Voronoi cells $\{\Omega_i\}$ of an optimal CVT generated by the isotropic CVT energy function $F(\mathbf{X})$ in Eq. (1) are asymptotically congruent regular hexagons. Gersho's conjecture has been proved in two dimensions by Gruber [1999] and supported by strong evidences in three dimensions (Du and Wang [2005]). Consequently, for an optimal CVT, the energy values $F_i(\mathbf{X})$ of all the CVT cells in Eq. (1) are asymptotically equal. Taking the dual of such a hexagonal mesh yields an isotropic triangle mesh with nearly equilateral triangle faces.

Anisotropic CVT. An anisotropic triangulation is computed with the CVT framework using a Riemannian metric in place of the Euclidean metric in the CVT energy function.

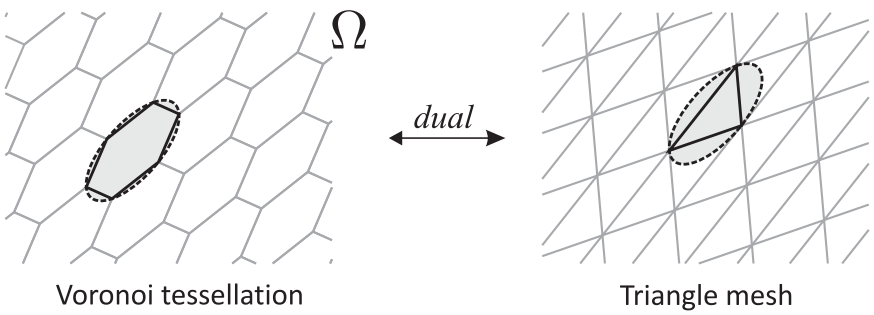

Figure 1: An anisotropic CVT and its dual triangulation.

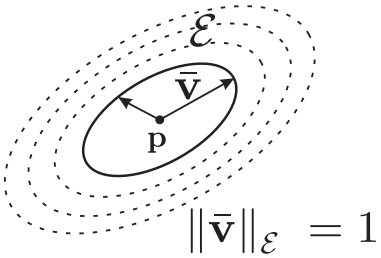

A Riemannian metric tensor M is defined by a positive definite quadratic form $Q(\mathbf{p};\mathbf{v}) = \mathbf{v}^t\mathbf{M}(\mathbf{p})\mathbf{v} : \mathcal{T}_\mathbf{p} \to \mathbb{R}$ in the two-dimensional tangent space $\mathcal{T}_\mathbf{p}$ of each point $\mathbf{p} \in \Omega$, where $\mathbf{v} \in \mathcal{T}_\mathbf{p}$. Since the metric M in $F_E(\mathbf{X})$ has an elliptic form, the iso-distance curves under this metric are ellipses centered at $\mathbf{p}$. The figure on the right shows the so-called *unit ellipse* $\mathcal{E} : \bar{\mathbf{v}}^T\mathbf{M}(\mathbf{p})\bar{\mathbf{v}} = 1$ (in solid line), on the tangent plane of a point $\mathbf{p}$, with the dashed lines being iso-distance curves which are called the *metric ellipses*. Equipped with the metric M, the domain Ω becomes a two-dimensional Riemannian manifold. Then the anisotropic CVT energy function is

$$F_E(\mathbf{X}) = \sum_{i=1}^{n} \int_{\Omega_i} d_E^2(\mathbf{x}, \mathbf{x}_i) \mathrm{d}\sigma \tag{2}$$

where $d_E(\mathbf{x}, \mathbf{y})$ is the geodesic distance between the points $\mathbf{x}$ and $\mathbf{y}$ on Ω with respect to the metric M, and Ω_i is the Voronoi cell of the seed $\mathbf{x}_i$ defined with respect to M. A CVT computed by minimizing $F_E(\mathbf{X})$ is an *anisotropic CVT*, since its Voronoi cells are elongated along the direction dictated by the metric M. To distinguish it from another type of anisotropic CVT we are going to introduce, we will call it the *elliptic CVT*. Similarly, we may define the stable elliptic CVT and the optimal elliptic CVT, corresponding to the local and global minimizers of $F_E(\mathbf{X})$, respectively. Taking the dual of an elliptic CVT yields an anisotropic triangulation (see Figure 1).

The shape of the Voronoi cells in an elliptic CVT can be deduced via the correspondence between an elliptic CVT of a two-dimensional Riemannian manifold Ω and an isotropic CVT of a two-dimensional manifold $\hat{\Omega}$ in some higher dimensional Euclidean space, which is established by Nash's embedding theorem (Nash [1956]). According to this correspondence (see Appendix A for details), within the corresponding tangent planes of Ω and $\hat{\Omega}$, a Voronoi cell of the elliptic CVT of a seed point $\mathbf{p} \in \Omega$ is locally the image under an affine mapping of a regular hexagonal Voronoi cell of the isotropic CVT of $\hat{\Omega}$. The linear part of this affine mapping is given by a matrix $\mathbf{G}$ such that $\mathbf{G}^T\mathbf{G} = \mathbf{M}^{-1}(\mathbf{p})$, where $\mathbf{M}(\mathbf{p})$ is the metric at $\mathbf{p}$. Hence, each Voronoi cell of an elliptic CVT of a seed $\mathbf{p}$ is asymptotically an *affinely regular hexagon* (i.e., a regular

hexagon under an affine mapping) inscribed to some metric ellipse $\mathcal{E}'$ at $\mathbf{p}$. Furthermore, the triangles in the dual anisotropic triangulation of an elliptic CVT have the same anisotropy defined by $\mathcal{E}'$ (see Figure 1).

Note that the factorization $\mathbf{G}^T\mathbf{G} = \mathbf{M}^{-1}(\mathbf{p})$ above is not unique, since there is also $(\mathbf{QG})^T(\mathbf{QG}) = \mathbf{M}^{-1}(\mathbf{p})$ for any orthogonal matrix $\mathbf{Q}$. It means that any affinely regular hexagonal regions H of different orientations inscribed to a metric ellipse at $\mathbf{p}$ in Ω corresponds to a regular hexgon (of different orientations) inscribed to the same metric circle in $\hat{\Omega}$. Since the embedding of Ω as $\hat{\Omega}$ preserves the CVT energy of each Voronoi cell, all H's of different orientations thus have the same elliptic CVT energy (Figure 2(a)). The elliptic CVT energy function $F_E(\mathbf{X})$ is therefore oblivious to the orientation of the Voronoi cells in an elliptic CVT and minimizing $F_E(\mathbf{X})$ does not have any control over the orientations of the anisotropic CVT cells that it generates.

The orientation of a Voronoi cell in an anisotropic CVT, however, can greatly affect the shape of the dual triangle. Figure 3 shows two sets of hexgonal cells with different orientations inscribed to some metric ellipse of the same anisotropy. It can be seen that while the cells in Figure 3(a) generate obtuse triangles in the dual mesh, those in Figure 3(b) yield acute triangles. Consequently, the lack of orientation control in an elliptic CVT generally leads to the larger number of obtuse triangles in the resulting anisotropic triangulation.

3. Hexagonal Minkowski metric

To enable the control of orientations of CVT cells, we introduce the *hexagonal Minkowski metric* in the CVT energy function. This metric is a special case of the Minkowski metric, also known as convex metric (Valentine [1964]). It can represent the same mesh anisotropy as the Riemannian metric *and* is sensitive to CVT cell orientations.

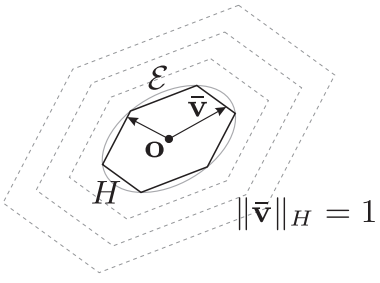

Given an ellipse $\mathcal{E}$ in $\mathbb{E}^2$ centered at the origin $\mathbf{o}$, let H be an affinely regular hexagon inscribed in $\mathcal{E}$ (see the figure on the right). The hexagon H defines a vector norm, denoted by $\|\mathbf{v}\|_H$, for vectors $\mathbf{v} \in \mathbb{R}^2$—$H$ is the "unit disk" in the sense that $\|\bar{\mathbf{v}}\|_H = 1$ for any vector $\bar{\mathbf{v}}$ on H, and $\|k\mathbf{v}\|_H = |k| \cdot \|\mathbf{v}\|_H$, $\forall k \in \mathbb{R}$ and $\forall \mathbf{v} \in \mathbb{E}^2$; hence, H is called a *unit hexagon*. The norm $\|\mathbf{v}\|_H$ will be called the *hexagonal Minkowski metric* or *HM metric* for short. For any two points $\mathbf{x}$ and $\mathbf{y}$ in $\mathbb{E}^2$, their distance induced by the HM metric is $d_H(\mathbf{x}, \mathbf{y}) = \|\mathbf{x} - \mathbf{y}\|_H$, and is called the *HM distance*. All the points $\mathbf{y}$ having the same HM distance to $\mathbf{x}$ lie on the same *metric hexagon* that is a uniformly scaled image of H centered at $\mathbf{x}$ (the dashed hexagons in the right figure).

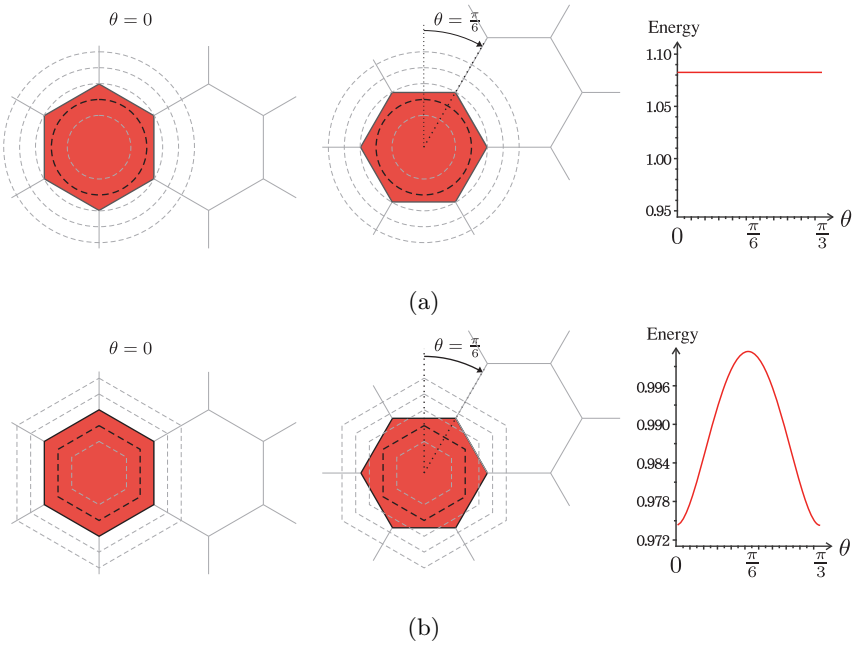

Figure 2: (a) The elliptic CVT energy remains constant for hexagonal cells with different orientations. (b) The HM CVT energy varies with the orientation of the hexagonal CVT cell. The dashed lines in black and in grey are the unit ellipse and metric ellipses in (a), and the unit hexagon and metric hexagons in (b), respectively.

The CVT energy function based on the HM metric, called the *HM CVT energy*, is defined as

$$F_H(\mathbf{X}) = \sum_{i=1}^{n} F_{H,i}(\mathbf{X}) = \sum_{i=1}^{n} \int_{\Omega_i} d_H^2(\mathbf{x}, \mathbf{x}_i) \mathrm{d}\sigma \tag{3}$$

The CVT computed by minimizing $F_H(\mathbf{X})$ will be called the HM CVT, which is a new kind of anisotropic CVT. Figure 2(b) shows that, the CVT energy $F_{H,i}(\mathbf{X}) \equiv \int_{\Omega_i} d_H^2(\mathbf{x}, \mathbf{x}_i) \mathrm{d}\sigma$ of a hexagonal cell Ω_i (in red) has different values when the CVT cell assumes different orientations. The energy reaches its minimum when the CVT cell has the same orientation as H. This suggests that we may control the orientation of CVT cells by minimizing the energy function $F_H(\mathbf{X})$ defined with an appropriate HM metric.

Let $\bar{F}_{\mathbf{c}}(s) = \int_{U(s,\mathbf{c})} d_H^2(\mathbf{x}, \mathbf{c}) \mathrm{d}\sigma$ denote the CVT energy of a seed $\mathbf{c}$ with a Voronoi cell $U(s, \mathbf{c})$ which is a uniformly scaled image of H centered at a point $\mathbf{c}$ and has area s. It is shown in Appendix B that $\bar{F}_{\mathbf{c}}(s)$ is indeed the minimum CVT energy among all regions of area s and that $\bar{F}_{\mathbf{c}}(s)$ is convex. Therefore, $F_H(\mathbf{X})$ has a lower bound $m\bar{F}_{\mathbf{c}}(\frac{|\Omega|}{m})$ when m, the number of seeds, is fixed. Moreover, when m approaches infinity, the affect due to the boundary of the domain Ω becomes negligible. The following theorem depicts the CVT pattern induced by the HM metric when the CVT energy $F_H(\mathbf{X})$ approaches its lower bound.

Theorem 1. *Let Ω be a convex compact region in $\mathbb{E}^2$ and $(\mathbf{X}_m)$ be a finite set of points in $\mathbb{E}^2$ with $|\mathbf{X}_m| = m$, for $m = 1, 2, \ldots$, such that*

$$F_H(\mathbf{X}_m) \sim m\bar{F}_{\mathbf{c}}(\frac{|\Omega|}{m}) \quad \textit{as} \quad m \to \infty,$$

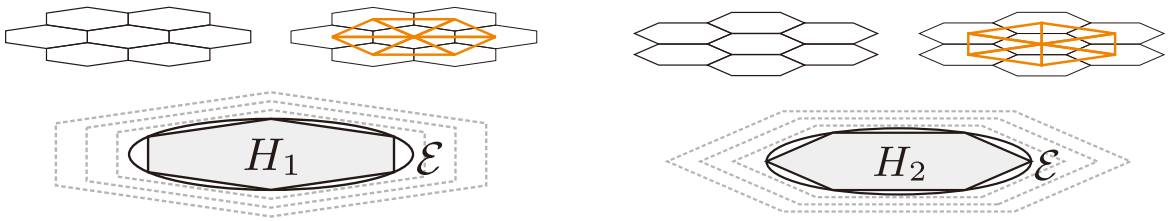

(a) (b)

Figure 3: (a) The CVT and its dual triangulation generated by the unit hexagon H_1. (b) The CVT and its dual triangulation generated by the unit hexagon H_2. It can be seen that the resulting triangle mesh contains obtuse triangles in (a) and contains acute triangles in (b).

where H is a regular hexagonal Minkowski metric. Then $\mathbf{X}_m$ is asymptotically a regular hexagonal pattern of edge length $(\frac{2|\Omega|}{3\sqrt{3}m})^{1/2}$, in which the hexagons are with the same orientation as H.

The proof is given in Appendix B.

We now consider choosing a unit hexagon to avoid obtuse triangles. Suppose that a part of a planar domain is endowed uniformly with HM metrics specified by the two unit hexagons H_1 and H_2 of different orientations as shown in Figure 3, respectively. As H_1 and H_2 are inscribed to the same metric ellipse, they define the same mesh anisotropy. It can be seen that the triangulation corresponding to H_1 consists of obtuse triangles (Figure 3(a)), while the triangulation corresponding to H_2 consists of acute triangles only (Figure 3(b)). Therefore in order to suppress obtuse triangles, we opt to use the unit hexagon H_2 in Figure 3(b), which is characterized by having one of its diagonals aligned with the major axis of the metric ellipse.

4. Algorithm

We assume the input is a domain Ω endowed with an HM metric tensor H, with proper orientations as shown in Figure 3(b) to suppress obtuse triangles. Our algorithm comprises the following steps:

Main Algorithm

Step 1: Initialization—Randomly distribute a set of n initial seeds $\mathbf{X} = \{\mathbf{x}_i\}$ on Ω.

Step 2: Perform an HM CVT optimization.

Step 3: Perform k passes of the following refinement step (or until a specific target reduction in the number of obtuse triangles is met):

3.1) Carry out an elliptic CVT optimization to cluster obtuse triangles.

3.2) Randomly perturb the seeds which are incident to obtuse triangles.

3.3) Carry out an HM CVT optimization to suppress obtuse triangles.

Step 4: Return the dual triangle mesh of the final optimized Voronoi tessellation as the resulting mesh.

Step 3 of the main algorithm serves to help the optimization to escape from a poor local minimum through perturbation, and hence to further reduce the number of obtuse triangles. This refinement step will be explained in detail in subsequent subsections.

Both the HM CVT and the elliptic CVT optimizations in the main algorithm are computed using the same framework as follows:

CVT optimization framework

Perform m iterations of the following optimization steps:

Step 1: Compute the Voronoi cells of $\mathbf{X}$, and the energy terms $F_i(\mathbf{X})$ and the gradient $\nabla F_i(\mathbf{X})$ of each seed $\mathbf{x}_i$.

Step 2: Use the L-BFGS method to obtain a new set of seeds $\mathbf{X}'$. Project $\mathbf{X}'$ to Ω. Replace $\mathbf{X}$ by $\mathbf{X}'$.

In the above CVT framework, the difference between computing an elliptic CVT and computing an HM CVT is that they use different ways of computing the Voronoi cells, the energy terms and the gradient terms, according to their respective metrics. This framework differs from the conventional CVT optimization framework in that instead of looping through until convergence of $F_i(\mathbf{X})$, we perform only a specific number of iterations (m) for the optimization steps out of efficiency consideration. The termination of the optimization is determined by the number of refinement steps taken in the main algorithm. Our implementation uses $m = 50$ iterations for all CVT optimizations which has demonstrated a satisfactory performance in our framework.

In the following we will present some implementation details of our method.

Computing Voronoi diagram. The existence of Delaunay triangulations on Riemannian manifolds has been established in Leibon and Letscher [2000], assuming sufficiently dense seeds. An anisotropic Voronoi diagram on a Riemannian manifold is so defined that the distance between points is given by the length of the shortest geodesics with respect to a Riemannian metric. To facilitate computation, this distance is usually approximated so that the bisectors between two seeds can be simplified as conic sections or quadric surfaces (Jiao et al. [2006]). Different methods for computing anisotropic Voronoi diagrams have been presented in Cheng et al. [2006], Labelle and Shewchuk [2003], Boissonnat et al. [2008]. However, no practical implementation of these methods are known that work for mesh surfaces.

Our method computes a discrete approximation of anisotropic Voronoi diagrams on a triangulation of the input domain Ω. The number of triangle elements of the input mesh needs to be high enough, as compared with the size of the output mesh, to ensure sufficient accuracy. A ratio of about $10:1$ is generally recommended. We also adopt the convention in Du and Wang [2005] in which the metric tensor is defined at the input mesh vertices.

To determine the Voronoi tessellation given seeds $\mathbf{X}$ on Ω, we compute an approximation to the Voronoi cell boundaries, each of which is the bisector of two seeds $\mathbf{x}_1$, $\mathbf{x}_2 \in \mathbf{X}$. A point $\mathbf{x} \in \Omega$ on the bisector has equal distances to $\mathbf{x}_1$ and $\mathbf{x}_2$, that is, $d_H(\mathbf{x}, \mathbf{x}_1) = d_H(\mathbf{x}, \mathbf{x}_2)$. Vertex-flooding as in Cohen-Steiner et al. [2004] is first used to label each vertex in Ω with its nearest seed point with respect to H. Our idea is to process each triangle T to locate any bisector that it may intersect.

For each triangle T, we locate the bisection points $\mathbf{z}_i$ on the sides of T whose endpoints have different labels using the bisection method (Figure 4). If the vertices of T are of three different labels, we first determine a bisecting line l equidistant to two seeds $\mathbf{x}_1$ and $\mathbf{x}_2$, and attempt to locate a Voronoi vertex $\mathbf{w}$ in T equidistant to all three seeds on l. If $\mathbf{w}$ is not in T, we shall seek its location in a neighbouring triangle T' (Figure 4(d)–(f)). Out of computational efficiency consideration, these treatments are not exhaustive and only serve to approximate the Voronoi boundaries.

Iterative solver. We use the limited memory BFGS method, also called the *L-BFGS method* (Liu et al. [2009]), to minimize the CVT energy function $F_H(\mathbf{X})$. The L-BFGS method is a variant of the classical BFGS, which is an iterative quasi-Newton method. The L-BFGS method takes as the input a set of seeds $\mathbf{X}$, the CVT energy $F_H(\mathbf{X})$ and its gradient $\nabla F_H(\mathbf{X})$, and returns the new positions for $\mathbf{X}$. To compute the CVT energy $F_{H,i}(\mathbf{X})$ of each Voronoi cell Ω_i, we use a triangulation $\mathcal{T}_i$ of Ω_i from the preceding computation

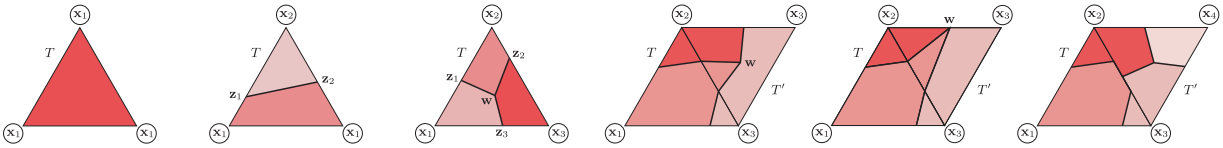

Figure 4: Computing the Voronoi cell boundaries in an input mesh triangle T. Each triangle vertex is labeled with its closest seed and L_T is the number of different labels at the vertices of T. (a) $L_T = 1$ and no boundary should lie in T. (b) $L_T = 2$ and the Voronoi cell boundary is a line connecting the bisection points on the edges of T. (c) $L_T = 3$ and a Voronoi cell vertex $\mathbf{w}$ is found in T. (d) If $\mathbf{w} \notin T$, we locate $\mathbf{w}$ on a neighbouring triangle T' with $L_{T'} = 2$. (e) Further if $\mathbf{w} \notin T'$, the tracking stops and $\mathbf{w}$ is snapped to an edge of T'. (f) The tracking also stops if $L_{T'} = 3$.

of the Voronoi diagram. Let $\triangle_j$ be a triangle in $\mathcal{T}_i$. The energy term $F_{H,i}(\mathbf{X})$ is approximated as:

$$F_{H,i}(\mathbf{X}) = \sum_{\triangle_j \in \mathcal{T}_i} \int_{\triangle_j} d_H^2(\mathbf{x}, \mathbf{x}_i) \mathrm{d}\sigma \approx \sum_{\triangle_j \in \mathcal{T}_i} f(\triangle_j)$$

where $f(\triangle_j)$ is the approximate CVT energy contributed by the triangle $\triangle_j$, given by the quadrature (Hillion [1977])

$$f(\triangle_j) = \frac{A_j}{3}\left(d_H^2(\mathbf{m}_1, \mathbf{x}_i) + d_H^2(\mathbf{m}_2, \mathbf{x}_i) + d_H^2(\mathbf{m}_3, \mathbf{x}_i)\right) \tag{4}$$

where A_j is the area of $\triangle_j$ and $\mathbf{m}_i$, $i = 1, 2, 3$, are the mid-points on the sides of $\triangle_j$. The gradient $\nabla F_H(\mathbf{X})$ is then computed approximately based on the expression of $f(\triangle_j)$ in Eq. (4).

Escaping from a poor local minimum. The optimization of the CVT energy function with the HM metric may be trapped at a poor local minimum which results in an undesirable CVT, as shown by the following theorem:

Definition 1 (Centrosymmetric Seed)**.** *A seed s is called a Centrosymmetric Seed (CS) if its neighbouring seeds (i.e., those seeds sharing at least one Voronoi edge with s) in the Voronoi diagram is centrosymmetric with respect to s. The right figure illustrates a CS s and its six neighbouring seeds in the dual triangulation.*

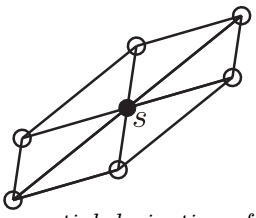

Theorem 2. *Given a set of seeds $\mathbf{Y}$, if $\mathbf{Y}$ consists of only centrosymmetric seeds, the partial derivative of $F_H(\mathbf{Y})$ with respect to each seed in $\mathbf{Y}$ is zero.*

The proof of the theorem is given in Appendix C.

Theorem 2 means that when a region R consists solely of CS, the gradient-based optimization of $F_H(\mathbf{X})$ cannot improve further locally in R due to the zero gradient. However, the CS seeds may be arranged in such a way that the dual triangulation of the CVT contains solely of obtuse triangles (as is shown in the

triangulation in Fig. 3(a)). We also observe that obtuse triangles often scatter over the domain after an HM CVT optimization, which renders it hard to further decrease the number of obtuse triangles due to the difficulty in fixing an isolated obtuse triangle in an optimization manner. Therefore, we devise a refinement step (Step 3 of the main algorithm) in order to keep the optimization from being trapped at such poor local minima. We note that the isotropic CVT energy function in a convex two-dimensional domain with C^2 density is proved to be C^2 smooth in Liu et al. [2009]. Elliptic CVT energy function with a unique elliptic metric inherits the C^2 smoothness and in this case the L-BGFS method converges faster. Also, elliptic CVT is shown to have the ability to cluster nearby obtuse triangles together by our experiments. Therefore, we use the elliptic CVT in an interleaved manner to cluster scattered obtuse triangles together to form connected regions of them. The positions of those seeds incident to an obtuse triangle are then randomly perturbed by at most 0.3 times the average length of their incident edges. Next, an HM CVT optimization is run again to obtain an enhanced result. Multiple passes of this refinement step can be performed if necessary. In this regard, our framework, apart from using a randomly distributed set of points on Ω as the initial seeds, may also accept a partial or complete remeshing result, such as that of an elliptic CVT of Ω as the input.

5. Validation

We first use an example to demonstrate the effectiveness of the HM metric in suppressing obtuse triangles. Figure 5(a) shows the triangulation of 1,000 seeds in a square computed with elliptic CVT, that is, by minimizing $F_E(\mathbf{X})$ in Eq. (2). The mesh has a uniform anisotropy of aspect ratio of $1:2$, and 40.6% of the triangles are obtuse (marked in blue). In comparison, the triangulation computed with the new HM CVT method (i.e., by minimizing $F_H(\mathbf{X})$ in Eq. (3)) has only 4.6% of its triangles being obtuse. Note that, due to boundary effects and difficulty in reaching a global minimum, the obtuse triangles in general cannot be removed completely.

Next, we present two examples for computing anisotropic triangulations using our algorithm as presented in Section 4. In the first example, we produce a triangulation of a two-dimensional domain with a vector field indicating the desired triangle alignments and elongations (Figure 6(a)). The input domain is of 56,644 triangles. An anisotropic metric tensor is defined based on the vector field shown in Figure 6(b). The elliptic CVT produces a mesh with 55.3% obtuse triangles (Figure 6(c)), which is greatly reduced to 17.1% by our method (Figure 6(d)). We use $k = 10$ passes of the refinement step in this example, and our method takes $426s$ for generating the triangulation.

Figure 7 shows a bone-like freeform surface for which the anisotropy metric M is defined to depend on the principal curvature directions and the principal curvature magnitudes. The ratio of the two eigenvalues of the metric M is the largest (about $5:1$) in the middle part of the bone. The input mesh is of 47,936

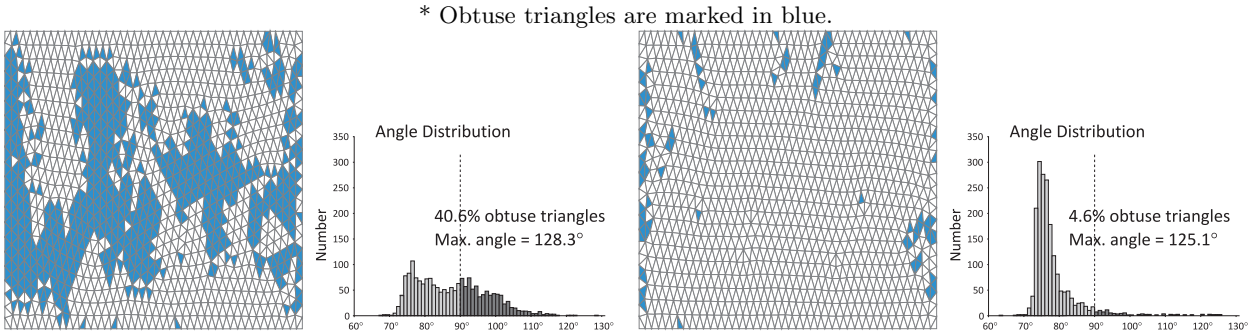

By Elliptic CVT (a)

By HM CVT (b)

Figure 5: Triangulation computed by (a) the elliptic CVT method; (b) the HM CVT method, of 1,000 vertices in a square with uniform anisotropy 1 : 2.

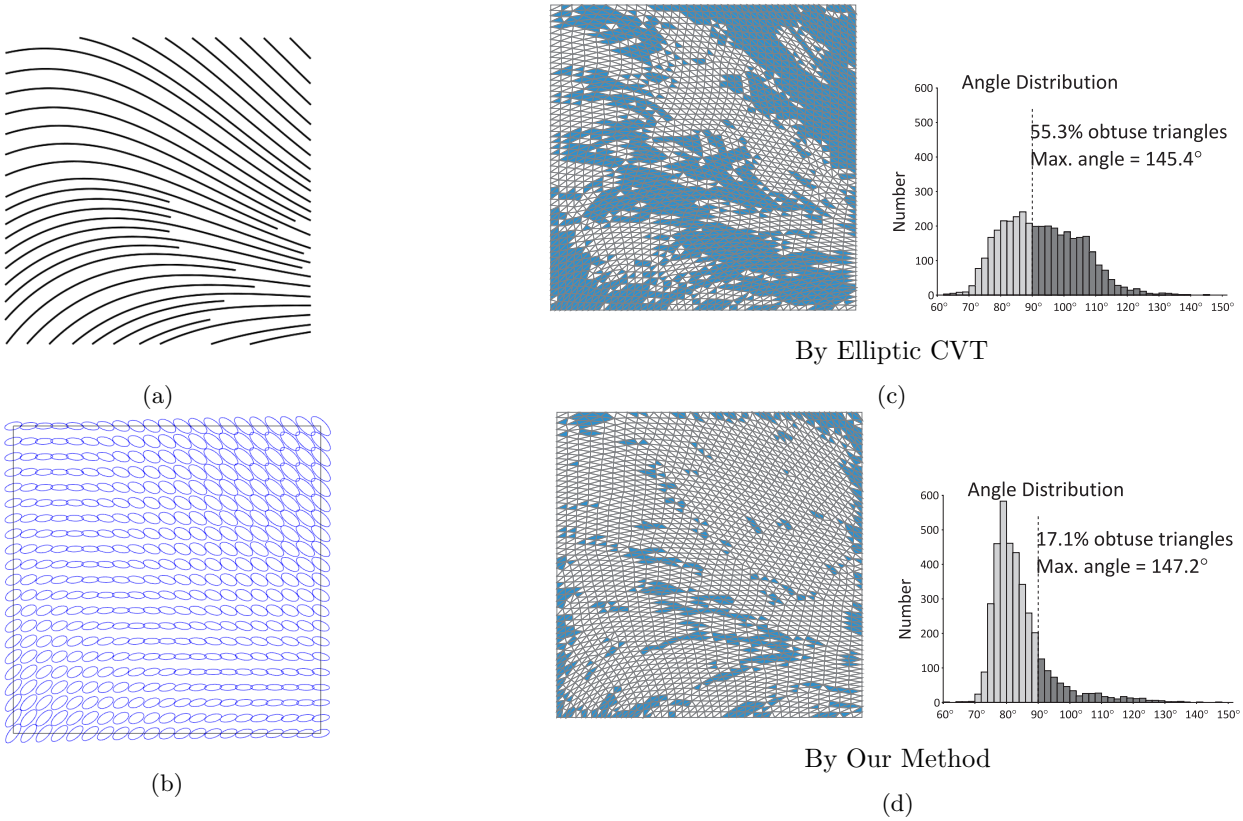

(a)

(b)

By Elliptic CVT (c)

By Our Method (d)

Figure 6: Triangulations of 2,000 points on a two-dimensional domain with varying anisotropy. (a) The input vector field. (b) An elliptic metric tensor is defined based on the vector field. (c) The elliptic CVT generates an anisotropic mesh with 55.3% obtuse triangles. (d) Our method generates an anisotropic mesh of the same anisotropy with 17.1% obtuse triangles. The meshes in (c) and (d) follow the same anisotropy defined in (b).

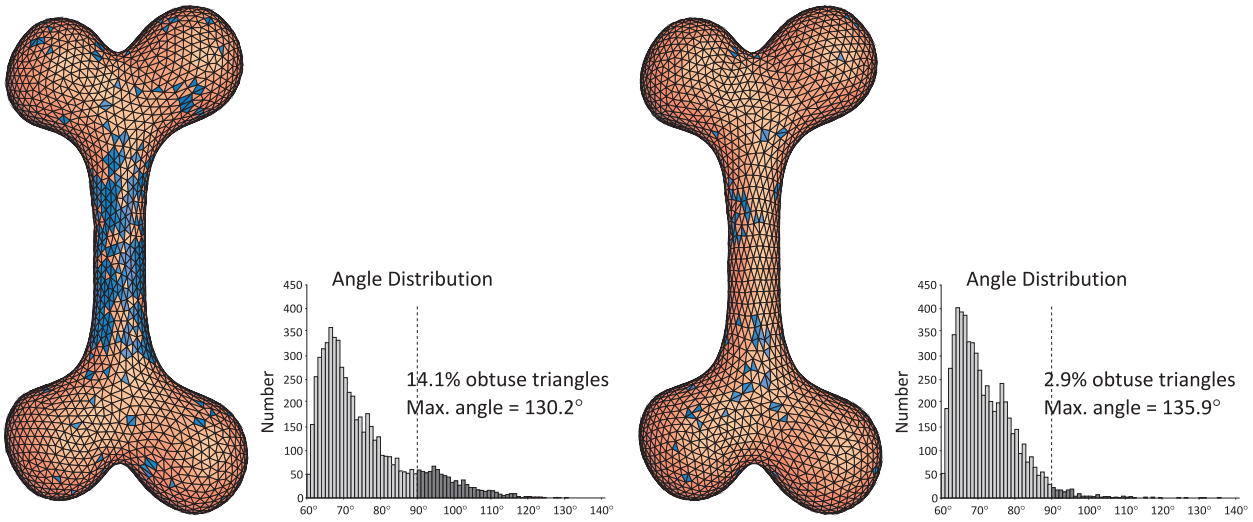

By Elliptic CVT (a)

By Our Method (b)

Figure 7: Anisotropic meshes of 3,000 vertices on a bone model. (a) The elliptic CVT generates a mesh with 14.1% obtuse triangles. (b) Our method generates a mesh with 2.9% obtuse triangles, using the result in (a) as the initial input.

triangles and a total of 3,000 seeds is used. The elliptic CVT results in 14.1% obtuse triangles which are mainly found on the bone shaft (Figure 7(a)). Our method based on the HM CVT produces a triangle mesh with 2.9% obtuse triangles (Figure 7(b)). The total time taken by our method is $412s$, using $k = 11$ passes of the refinement steps.

6. Conclusions

Our method can greatly reduce the number of obtuse triangles in anisotropic meshes, as compared with the conventional CVT-based method. However, because our method is an optimization method, it does not have the ability to reduce the maximal angle. Besides that, it still cannot remove obtuse triangles completely. There are at least two reasons for this. The first is the boundary effect, that is, obtuse triangles tend to persist along domain boundaries, as shown in the examples in Figures 5 and 6. The second reason is the difficulty in reaching the global minimizer of the HM CVT energy function, despite our careful optimization strategy that has kept us from getting trapped in poor local minima. Hence, further research is needed to improve the result of the optimization.

Another issue is efficiency. Our current implementation needs several minutes to compute a mesh of moderate size (several thousand vertices). While slow convergence in CVT computation is certainly a factor, we note that in each iteration, most of the time is spent on computing the anisotropic Voronoi diagram on a mesh.

It is envisioned that considerable speedup might be achieved by using surface parameterization with multi-charts and GPU acceleration for computing anisotropic Voronoi diagrams.

I. Babuska and A. K. Aziz. On the angle condition in the finite element method. *SIAM Journal on Numerical Analysis*, 13 (2):214–226, 1976.

Brenda Baker, Eric Grosse, and Conor Rafferty. Nonobtuse triangulation of polygons. *Journal Discrete and Computational Geometry*, 3(1):147–168, 1988.

Marshall Wayne Bern and David Eppstein. Mesh generation and optimal triangulation. In Ding-Zhu Du and Frank Kwang-Ming Hwang, editors, *Computing in Euclidean Geometry*, number 1 in Lecture Notes Series on Computing, pages 23–90. World Scientific, 1992a.

Marshall Wayne Bern and David Eppstein. Polynomial-size non-obtuse triangulation of polygons. *International Journal of Computational Geometry & Applications*, 2(3):241–255, September 1992b. Special issue for 7th SCG.

J-D. Boissonnat, C. Wormser, and M. Yvinec. Locally uniform anisotropic meshing. In *Symposium on Computational Geometry (SOCG)*, pages 270–277, 2008.

Frank J. Bossen and Paul S. Heckbert. A pliant method for anisotropic mesh generation. In *Proceedings of the 5th International Meshing Roundtable*, pages 173–190, 1996.

J. Brandts, S. Korotov, M. Krizek, and J. Solc. On nonobtuse simplicial partitions. *SIAM Review*, 51:317–335, January 2009. doi: 10.1137/060669073.

Siu-Wing Cheng, Tamal K. Dey, Edgar A. Ramos, and Rephael Wenger. Anisotropic surface meshing. In *Proceedings of the Seventeenth Annual ACM-SIAM Symposium on Discrete Algorithms, SODA 2006*, pages 202–211, 2006.

David Cohen-Steiner, Pierre Alliez, and Mathieu Desbrun. Variational shape approximation. *ACM Transactions on Graphics (Proceeding of SIGGRAPH 2004)*, 23(3):905–914, 2004.

Tamal Dey, Joshua Levine, and Rephael Wenger. A Delaunay simplification algorithm for vector fields. In *PG '07: Proceedings of the 15th Pacific Conference on Computer Graphics and Applications*, pages 281–290, 2007.

Q. Du, Z. Huang, and D. Wang. Mesh and solver co-adaptation in finite element methods for anisotropic problems. *Numerical Methods for Partial Differential Equations*, 21:859–874, 2005.

Qiang Du and Desheng Wang. Anisotropic centroidal Voronoi tessellations and their applications. *SIAM J. Sci. Comput.*, 26 (3):737–761, 2005.

Qiang Du, Vance Faber, and Max Gunzburger. Centroidal Voronoi tessellations: applications and algorithms. *SIAM Review*, 41:637–676, 1999.

N. Dyn, , David Levin, and S. Rippa. Data dependent triangulations for piecewise linear interpolation. *IMA Journal of Numerical Analysis*, 10(1):137–154, 1990.

Nira Dyn, Kai Hormann, Sun-Jeong Kim, and David Levin. Optimizing 3D triangulations using discrete curvature analysis. pages 135–146, 2001.

A. Gersho. Asymptotically optimal block quantization. *Information Theory, IEEE Transactions on*, 25(4):373–380, Jul 1979. ISSN 0018-9448.

Peter M. Gruber. A short analytic proof of Fejes Tóth's theorem on sums of moments. *Aequationes Mathematicae*, 58:291–295, 1999.

Peter M. Gruber. Optimal configurations of finite sets in Riemannian 2-manifolds. *Geometriae Dedicata*, 84:271–320, 2001.

Pierre Hillion. Numerical integration on a triangle. *International Journal for Numerical Methods in Engineering*, 11:797–815, 1977.

Xiangmin Jiao, Andrew Colombi, Xinlai Ni, and John C. Hart. Anisotropic mesh adaptation for evolving triangulated surfaces. In *Proceedings of the 15th International Meshing Roundtable*, pages 173–190, 2006.

Francois Labelle and Jonathan Richard Shewchuk. Anisotropic Voronoi diagrams and guaranteed-quality anisotropic mesh

generation. In *Proceedings of the nineteenth annual symposium on computational geometry (SCG 03)*, pages 191–200, 2003.

Greg Leibon and David Letscher. Delaunay triangulations and Voronoi diagrams for Riemannian manifolds. In *SCG '00: Proceedings of the sixteenth annual symposium on computational geometry*, pages 341–349, 2000.

J. Y. S. Li and H. Zhang. Nonobtuse remeshing and mesh decimation. In *Symposium on Geometry Processing*, pages 235–238, 2006.

Yang Liu, Wenping Wang, Bruno Lévy, Feng Sun, Dong-Ming Yan, Lin Lu, and Chenglei Yang. On centroidal Voronoi tessellation—energy smoothness and fast computation. *ACM Trans. Graph.*, 28(4):1–17, 2009.

John Nash. The imbedding problem for Riemannian manifolds. *The Annals of Mathematics*, 63(1):20–63, 1956.

Shmuel Rippa. Long and thin triangles can be good for linear interpolation. *SIAM Journal on Numerical Analysis*, 29(1): 257–270, 1992.

Jonathan Richard Shewchuk. What is a good linear element? Interpolation, conditioning, and quality measures. In *Proceedings of the 11th International Meshing Roundtable*, pages 115–126, 2002.

Kenji Shimada. Anisotropic triangular meshing of parametric surfaces via close packing of ellipsoidal bubbles. In *Proceedings of the 6th International Meshing Roundtable*, pages 375–390, 1997.

R. Simpson. Anisotropic mesh transformations and optimal error control. *Applied Numer. Math.*, 14(1-3):183–198, 1994.

Frederick A. Valentine. *Convex Sets*. McGraw-Hill, New York, 1964.

Sébastien Valette, Jean-Marc Chassery, and Rémy Prost. Generic remeshing of 3D triangular meshes with metric-dependent discrete Voronoi diagrams. *IEEE Transactions on Visualization and Computer Graphics*, 14(2):369–381, 2008.

Desheng Wang and Qiang Du. Mesh optimization based on the centroidal Voronoi tessellation. *International Journal of Numerical Analysis and Modeling*, 2:100–113, 2005.

Appendix A. Correspondence between an ACVT of a two-dimensional manifold and a CVT of a higher dimensional Euclidean space

Here we will discuss how the shape of a Voronoi cell of an optimal anisotropic CVT (or ACVT) is determined by a Riemannian metric M. First we will establish the correspondence between an ACVT on a two-dimensional Riemannian manifold Ω and an isotropic CVT in a higher dimensional Euclidean space. According to Nash's embedding theorem (Nash [1956]), the surface Ω, as a two-dimensional Riemannian manifold, can be embedded isometrically as a two-dimensional manifold $\hat{\Omega}$ in a Euclidean space $\mathbb{E}^k$, which is not necessarily three-dimensional—that is, $\hat{\Omega} \subset \mathbb{E}^k$ is equipped with Euclidean metric. Denote this mapping (or embedding) by $R(\mathbf{x}) = \hat{\mathbf{x}}$: $\Omega \to \hat{\Omega}$. Clearly, R maps the original anisotropic CVT function $F(\mathbf{X})$ in Eq. (2) to

$$\hat{F}(\hat{X}) = \sum_{i=1}^{n} \int_{\hat{\Omega}_i} d_E^2(\hat{\mathbf{x}}, \hat{\mathbf{x}}_i) \mathrm{d}\sigma,$$

which is the conventional CVT function on $\hat{\Omega}$ with Euclidean metric. It follows that $\hat{F}_i(\hat{X}) \equiv F_i(X)$ for all i and $\hat{F}(\hat{X}) \equiv F(X)$. Hence, the minimization of $F(\mathbf{X})$ is equivalent to that of $\hat{F}(\hat{\mathbf{X}})$ under R.

As proved in Gruber [2001], the Voronoi cell $\hat{\Omega}_i$ of the CVT on the two-dimensional manifold $\hat{\Omega}$ with Euclidean metric is asymptotically a regular hexagon $\hat{H}$. Let H and $\hat{H}$ be corresponding optimal CVTs on

Ω and $\hat{\Omega}$. Consider the corresponding seeds $\mathbf{x}_i$ of H and $\hat{\mathbf{x}}_i$ of $\hat{H}$. Between the tangent spaces $\mathcal{T}_i$ of Ω at $\mathbf{x}_i$ and $\hat{\mathcal{T}}_i$ of $\hat{\Omega}$ at $\hat{\mathbf{x}}_i$, the metric $M(\mathbf{x}_i) = (G^{-1})^T G^{-1}$ at $\mathbf{x}_i$ induces a linear mapping $\mathbf{v} = G\hat{\mathbf{v}} : \hat{\mathcal{T}}_i \to \mathcal{T}_i$, which is the linearization of the stretching of the embedding $R(\mathbf{x})$ of Ω as $\hat{\Omega}$. The linear mapping G^{-1} maps the regular hexagonal Voronoi cell $\hat{\mathbf{H}}$ of the CVT at $\hat{\mathbf{x}}_i$ to an affinely scaled (anisotropic) hexagonal cell $\mathbf{H}$ of the ACVT at $\mathbf{x}_i$, which is inscribed in the ellipse $\mathbf{v}^t M \mathbf{v} = c$ in the tangent plane $\mathcal{T}_i$, for some constant $c > 0$. Thus, we have determined asymptotically the shape the Voronoi cells of a CVT produced by the anisotropic CVT energy function $F(\mathbf{X})$ in Eq. (2). Furthermore, because $\hat{F}_i(\hat{X}) \equiv F_i(X)$ for all i, it follows from the isotropic case that the anisotropic CVT energy terms $F_i(\mathbf{X})$ are equal for all i asymptotically in an optimal anisotropic CVT.

Appendix B. Proof of Theorem 1

Appendix B.1. The Result

Let us define the following notations that will be used in the proof:

- H: a regular hexagonal Minkowski metric. It also takes the meaning of the unit disk, that is, the unit hexagon, in the metric H, when the context is clear.
- $U(s, \mathbf{c})$: a region which is a uniformly scaled image of H centered at a point $\mathbf{c}$ and has area s.
- $F_{\mathbf{c}}(R) = \int_R d_H^2(\mathbf{x}, \mathbf{c}) \mathrm{d}\sigma$: the HM CVT energy of a seed $\mathbf{c}$ with R as its Voronoi cell.
- $\bar{F}_{\mathbf{c}}(s) = \int_{U(s,\mathbf{c})} d_H^2(\mathbf{x}, \mathbf{c}) \mathrm{d}\sigma$: the HM CVT energy of a seed $\mathbf{c}$ with a Voronoi cell $U(s, \mathbf{c})$.
- $F_{min}(s, i)$: the minimal HM CVT energy of all possible Voronoi cells of area s having i neighbours.

Theorem 1. *Let Ω be a convex compact region in $\mathbb{E}^2$ and $\left(\mathbf{X}_m\right)$ be a finite set of points in $\mathbb{E}^2$ with $|\mathbf{X}_m| = m$, for $m = 1, 2, \ldots,$ such that*

$$F_H(\mathbf{X}_m) \sim m\bar{F}_{\mathbf{c}}(\frac{|\Omega|}{m}) \quad as \quad m \to \infty,$$

where H is a regular hexagonal Minkowski metric, then $\mathbf{X}_m$ is asymptotically a regular hexagonal pattern of edge length $(\frac{2|\Omega|}{3\sqrt{3}m})^{1/2}$, in which the hexagons are with the same orientation as H.

The statement of Theorem 1 is similar to the statement of the celebrated two-dimensional Gersho's conjecture (Gersho [1979]) which is proved in Gruber [1999].

The outline of the proof of Theorem 1, which is inspired by Gruber [2001], is given here. We emphasize that all Voronoi cells mentioned in Appendix B is induced by the regular hexagonal Minkowski metric H in Theorem 1. First, we show that most Voronoi cells are completely inside Ω by Lemma 8. Then, we have Lemma 12 showing that most Voronoi cells have six neighbours. Also, Lemma 13 shows that most

Voronoi cells have the same area, with an $o(\frac{|\Omega|}{m})$ error. Finally, by Lemma 14 we show that most Voronoi cells assume a regular hexagonal shape with the same orientation as H; that is, the area of the boolean difference of the Voronoi cell Ω_i of a seed $\mathbf{x}_i$ and $U(|\Omega_i|, \mathbf{x}_i)$ is $o(|\Omega_i|)$. By employing the nice property that under the regular hexagonal Minkowski metric, the Voronoi cell realizing the smallest energy for a given seed is a regular hexagon, not a disk, we give a new result in Lemma 11. This result is the key in the proofs of Lemma 12, 13 and 14; the three proofs are fundamentally different from the proofs in Gruber [2001].

If a Voronoi cell has an intersection with the boundary of Ω, its number of neighbours is added by 1, that is, we also count $\bar{\Omega}$, the complement of Ω, as a neighbour. The number of Voronoi cells with i neighbours is denoted as m_i, $i = 3, 4, \ldots, k$, where k is the maximal i with $m_i > 0$. All Voronoi cells with i neighbours are labelled as D_{ij}, $i = 3, 4, \ldots, k$ and $j = 1, 2, \ldots, m_i$. The area of D_{ij} is denoted by $|D_{ij}|$. Without loss of generality, we suppose that $|\Omega| = 1$. It is easy to see that

$$|D_{31}| + |D_{32}| + \ldots + |D_{3m_3}| + \ldots + |D_{km_k}| = 1. \tag{B.1}$$

Appendix B.2. The Proof

Lemma 2. *Consider the HM CVT energy term $F_{\mathbf{c}}(R) = \int_R d_H^2(\mathbf{x}, \mathbf{c})\mathrm{d}\sigma$ of a compact region R in $\mathbb{E}^2$, where $\mathbf{c}$ is a fixed point. Among all the compact regions of some fixed area s_0, $F_{\mathbf{c}}(R)$ has a unique minimizer $U(s_0, \mathbf{c})$ which is a uniformly scaled image of H centered at $\mathbf{c}$.*

Proof. Without loss of generality, suppose that $\mathbf{c}$ is at the origin $\mathbf{o}$. Suppose that R_0 is the minimizer of $F_{\mathbf{c}}(R)$ among all the compact regions of area s_0. Then there is a scaled image $R_1 = k_1 R_0$ of R_0, for some $k_1 > 0$, that has the same area of the unit hexagon H, which is $k_1^2 s_0$. It follows that R_1 is the minimizer of $F_{\mathbf{c}}(R)$ among all compact regions of area $k_1^2 s_0$, since $F_{\mathbf{c}}(k_1 R) = k_1^4 F_{\mathbf{c}}(R)$ for any R.

Now we are going to prove by contradiction that $R_1 = H$. Assume $R_1 \neq H$. Since R_1 and H have equal area, $R_1 \backslash H \neq \emptyset$ and $H \backslash R_1 \neq \emptyset$. Therefore, we can remove a region D_1 of sufficiently small area from $R_1 \backslash H$ and add a region D_2 of the same area of D_1 from $H \backslash R_1$ to form $R_2 = (R_1 \backslash D_1) \bigcup D_2$ (See the right figure). Clearly, R_2 and R_1 have equal area $k_1^2 s_0$. Since D_2 is inside H and D_1 is outside H, $d_H(\mathbf{x}, \mathbf{o}) < 1 < d_H(\mathbf{y}, \mathbf{o})$, $\forall \mathbf{x} \in D_2$ and $\forall \mathbf{y} \in D_1$. It follows that

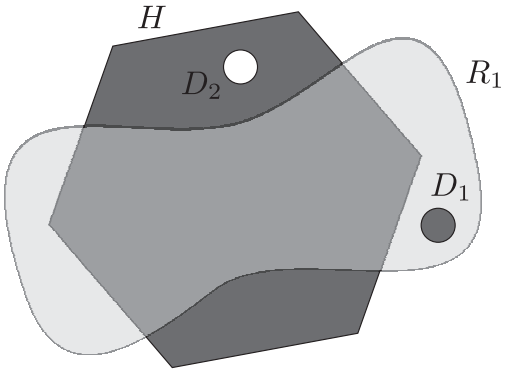

$$F_{\mathbf{c}}(R_2) = F_{\mathbf{c}}(R_1) - F_{\mathbf{c}}(D_1) + F_{\mathbf{c}}(D_2) < F_{\mathbf{c}}(R_1).$$

This contradicts that R_1 is the minimizer of $F_{\mathbf{c}}(R)$ among all the compact regions of area $k_1^2 s_0$. Therefore, $R_1 = H$. Hence, $R_0 = k_1^{-1} R_1 = k_1^{-1} H$, that is, R_0 is a uniformly scaled image of H. This completes the proof. □

Corollary 3. *The HM CVT energy* $\bar{F}_{\mathbf{c}}(s) = \int_{U(s,\mathbf{c})} d_H^2(\mathbf{x}, \mathbf{c}) \mathrm{d}\sigma$ *of a seed* $\mathbf{c}$ *with a Voronoi cell which is a uniformly scaled image of* H *centered at* $\mathbf{c}$ *of area* s *gives the minimum energy among all Voronoi cells of area* s*.*

Lemma 4. $\bar{F}_{\mathbf{c}}(s)$ *is strictly convex, that is,*

$$\lambda \bar{F}_{\mathbf{c}}(s_1) + (1-\lambda)\bar{F}_{\mathbf{c}}(s_2) > \bar{F}_{\mathbf{c}}(\lambda s_1 + (1-\lambda)s_2)$$

for any distinct $s_1, s_2 > 0$ *and* $\lambda \in (0,1)$*.*

Proof. $\bar{F}_{\mathbf{c}}(s) = \frac{\sqrt{3}}{12} s^2$, which can be easily derived with integration by substitution. Therefore, $\bar{F}_c(s)$ is strictly convex. □

Lemma 5. *For each* σ *with* $0 < \sigma < 1$*, there exists* $\tau > 1$ *such that for each* $s > 0$ *and for all positive* m*,*

$$\sigma m \bar{F}_{\mathbf{c}}(\frac{s}{\sigma m}) \geq \tau m \bar{F}_{\mathbf{c}}(\frac{s}{m})$$

holds.

Proof. Since $\bar{F}_{\mathbf{c}}(s) = \frac{\sqrt{3}}{12} s^2$, we have $\bar{F}_{\mathbf{c}}(ks) = k^2 \bar{F}_{\mathbf{c}}(s)$. Therefore, $\sigma m \bar{F}_{\mathbf{c}}(\frac{s}{\sigma m}) = \frac{\sigma m}{\sigma^2} \bar{F}_{\mathbf{c}}(\frac{s}{m}) = \frac{m}{\sigma} \bar{F}_{\mathbf{c}}(\frac{s}{m})$. By choosing $\tau \in (1, \frac{1}{\sigma}]$, we then have $\sigma m \bar{F}_{\mathbf{c}}(\frac{s}{\sigma m}) \geq \tau m \bar{F}_{\mathbf{c}}(\frac{s}{m})$. □

Lemma 6. *Let* Ω *be a convex compact region in* $\mathbb{E}^2$ *and* $\left(\mathbf{X}_m\right)$ *be a sequence of finite sets in* $\mathbb{E}^2$ *with* $|\mathbf{X}_m| = m$*, for* $m = 1, 2, \ldots$*, such that*

$$F_H(\mathbf{X}_m) \sim m \bar{F}_{\mathbf{c}}(\frac{|\Omega|}{m}) \quad as \quad m \to \infty.$$

Then we have $max_{\mathbf{p} \in \mathbf{X}_m} \{diam\big(VC(\mathbf{p}) \bigcap int(\Omega)\big)\} \sim 0$ *as* $m \to \infty$*, where* $diam(R)$ *and* $int(R)$ *denote the diameter and the interior of a region* R*, respectively, and* $VC(\mathbf{p})$ *denotes the Voronoi cell of a seed* $\mathbf{p}$*.*

Proof. To prove the lemma, we need only to show that given any $\epsilon > 0$, for all sufficiently large m, $\forall \mathbf{p} \in \mathbf{X}_m$ and $\mathbf{x} \in VC(\mathbf{p}) \bigcap int(\Omega)$, the distance between $\mathbf{x}$ and $\mathbf{p}$ is less than 2ϵ. Now, the compactness of the closure of $int(\Omega)$ implies that there are finitely many points in $int(\Omega)$ whose ϵ-neighbourhoods cover $int(\Omega)$. When m is sufficiently large, each of these ϵ-neighbourhoods contains at least one point of $\mathbf{X}_m$. Otherwise, there is a contradiction that the integral $F_H(\mathbf{X}_m)$ does not converge to 0. To show this, assume there exists a point q whose ϵ-neighbourhood does not contain any point of $\mathbf{X}_m$. We then compute the integral $F_H(\mathbf{X}_m)$ over the domain D, where D is a disk centered at q with radius $\frac{\epsilon}{2}$. It is easy to see that the distance between any point in D and its nearest point in $\mathbf{X}_m$ is no less than a constant $c_1 = \frac{\epsilon}{2}$ and the area of D is also a

constant $c_2 = \frac{\pi\epsilon^2}{4}$. The integral $F_H(\mathbf{X}_m)$ over the domain D is then a constant and therefore the integral $F_H(\mathbf{X}_m)$ does not converge to 0. However, $m\bar{F}_{\mathbf{c}}(\frac{|\Omega|}{m}) = \frac{1}{m}\bar{F}_{\mathbf{c}}(|\Omega|)$, which converges to 0. Therefore, for each $\mathbf{x} \in int(\Omega)$, the nearest point in $\mathbf{X}_m$ to $\mathbf{x}$ has a distance less than 2ϵ from $\mathbf{x}$. Furthermore, for each $\mathbf{x} \in VC(\mathbf{p}) \bigcap int(\Omega)$, the point $\mathbf{p}$ is (one of) the nearest point(s) in $\mathbf{X}_m$ to $\mathbf{x}$, we thus have the distance between $\mathbf{x}$ and $\mathbf{p}$ is less than 2ϵ. This concludes the proof. □

Lemma 7 and Lemma 8 show that most Voronoi cells are in the interior of Ω.

Lemma 7.

$$(m + o(m))\bar{F}_{\mathbf{c}}(\frac{1}{m}) \geq F_{min}(|D_{31}|, 3) + F_{min}(|D_{32}|, 3) + \ldots + F_{min}(|D_{3m_3}|, 3) + \ldots + F_{min}(|D_{km_k}|, k),$$

where $o(m)$ is a quantity dominated by m.

Proof. Under the assumption in Theorem 1,

$$\begin{aligned}(m + o(m))\bar{F}_{\mathbf{c}}(\frac{1}{m}) &\geq F_H(\mathbf{X}_m) \\ &= \sum_{i=3}^{k}\sum_{j=1}^{m_i} F_{D_{ij}}(\mathbf{X}_m) \\ &= F_{D_{31}}(\mathbf{X}_m) + F_{D_{32}}(\mathbf{X}_m) + \ldots + F_{D_{3m_3}}(\mathbf{X}_m) + \ldots + F_{D_{km_k}}(\mathbf{X}_m) \\ &\geq F_{min}(|D_{31}|, 3) + F_{min}(|D_{32}|, 3) + \ldots + F_{min}(|D_{3m_3}|, 3) \\ &\quad + \ldots + F_{min}(|D_{km_k}|, k).\end{aligned}$$

□

Lemma 8.

$$\begin{aligned}m_{int} &= |\{D_{ij} \mid D_{ij} \subseteq int(\Omega)\}| \\ &= m - o(m), \quad as \quad m \to \infty.\end{aligned}$$

Proof. If this is not the case, then we have $m_{int} \leq \sigma^2 m$ for infinitely many m which constitute a sequence, where $0 < \sigma < 1$. Let $\tau = \chi^2 > 1$ be the same τ as stated in Lemma 5. Also, we choose a suitable χ such that $\chi \leq \frac{1}{\sigma}$. Since $(m + o(m))\bar{F}_{\mathbf{c}}(\frac{1}{m}) \to 0$ as $m \to \infty$, by Lemma 6, we have $max_{i,j}\{diam(D_{ij})\} \to 0$ as $m \to \infty$. Choose $K \subset int(\Omega)$ which is homothetic to Ω with $|K| = |\Omega|/\chi = 1/\chi$. Then for all sufficiently large m, there are $m_K \leq m_{int}$ Voronoi cells which have nonempty intersection with K. Thus we have the

following contradiction:

$$
\begin{aligned}
&\big(m+o(m)\big)\bar{F}_{\mathbf{c}}(\frac{1}{m}) \\
&\quad\geq F_{min}(|D_{31}|,3)+F_{min}(|D_{32}|,3)+\ldots+F_{min}(|D_{3m_3}|,3)+\ldots+F_{min}(|D_{km_k}|,k) \\
&\quad\geq F_{min}(|D_{31}\cap K|,3)+F_{min}(|D_{32}\cap K|,3)+\ldots+F_{min}(|D_{3m_3}\cap K|,3) \\
&\qquad\quad +\ldots+F_{min}(|D_{km_k}\cap K|,k) \\
&\quad\geq \bar{F}_{\mathbf{c}}(|D_{31}\cap K|)+\bar{F}_{\mathbf{c}}(|D_{32}\cap K|)+\ldots+\bar{F}_{\mathbf{c}}(|D_{3m_3}\cap K|) \\
&\qquad\quad +\ldots+\bar{F}_{\mathbf{c}}(|D_{km_k}\cap K|) \\
&\quad\geq m_K\bar{F}_{\mathbf{c}}(\frac{|K|}{m_K}) \\
&\quad\geq m_{int}\bar{F}_{\mathbf{c}}(\frac{|K|}{m_{int}}) \\
&\quad= \frac{1}{\chi}\chi m_{int}\bar{F}_{\mathbf{c}}(\frac{1}{\chi m_{int}})\geq\frac{1}{\chi}\chi\sigma^2 m\bar{F}_{\mathbf{c}}(\frac{1}{\chi\sigma^2 m})\geq\frac{1}{\chi}\sigma m\bar{F}_{\mathbf{c}}(\frac{1}{\sigma m})\geq\frac{\tau}{\chi}m\bar{F}_{\mathbf{c}}(\frac{1}{m})=\chi m\bar{F}_{\mathbf{c}}(\frac{1}{m}).
\end{aligned}
$$

□

Lemma 9.

$$3m_3+4m_4+\ldots+km_k=6(m_3+m_4+\ldots+m_k)-o(m)=6m-o(m).$$

Proof. We consider the Voronoi tessellation of $\mathbf{X}_m$ in Ω induced by the HM metric H as a graph G. We denote v, e, n as the number of vertices, edges, and faces of G, respectively. It is trivial that G is planar since it corresponds to a planar tiling of a convex region Ω. Hence, we have $3v = 3m_3 + 4m_4 + \ldots + km_k + v_{bd}$, where v_{bd} is the number of points in $\mathbf{X}_m$ whose Voronoi cells have an intersection with the boundary of Ω. We also have $2e = 3m_3 + 4m_4 + \ldots + km_k + e_{bd}$, where e_{bd} is the number of Voronoi edges which have intersections with the boundary of Ω.

By Euler's formula on planar graph, we have $6 = 6v-6e+6n = -(3m_3+4m_4+...+km_k)+6n+2v_{bd}-3e_{bd}$. Since we assume all points in $\mathbf{X}_m$ are in Ω, we have $n = m$; and $2v_{bd} - 3e_{bd} - 6 = o(m)$ from Lemma 8. This completes the proof. □

Lemma 10. *Given a seed* $\mathbf{c}$ *and its Voronoi region* R *with area* s*, if the area of* $R\setminus U(s,\mathbf{c})$ *(i.e.,the boolean difference of* R *and* $U(s,\mathbf{c})$*) is* αs*, where* α *is a positive constant, then we have* $F_{\mathbf{c}}(R)\geq\theta\bar{F}_{\mathbf{c}}(s)$*, where* $\theta>1$ *is a constant.*

Proof. We partition the region R into two parts R_{in} and R_{out}, where $R_{in} = R\cap U(s,\mathbf{c})$ and $R_{out} = R - R_{in}$.

Then,

$$\begin{aligned} F_{\mathbf{c}}(R) &= F_{\mathbf{c}}(R_{in}) + F_{\mathbf{c}}(R_{out}) \\ &= F_{\mathbf{c}}(R_{in}) + F_{\mathbf{c}}(R_{out} \cup U(s,\mathbf{c})) - F_{\mathbf{c}}(U(s,\mathbf{c})) \\ &\geq \bar{F}_{\mathbf{c}}((1-\alpha)s) + \bar{F}_{\mathbf{c}}((1+\alpha)s) - \bar{F}_{\mathbf{c}}(s) \\ &= (1-\alpha)^2\bar{F}_{\mathbf{c}}(s) + (1+\alpha)^2\bar{F}_{\mathbf{c}}(s) - \bar{F}_{\mathbf{c}}(s) \\ &= (1+2\alpha^2)\bar{F}_{\mathbf{c}}(s). \end{aligned}$$

We have $\theta = 1 + 2\alpha^2$ to finish the proof. □

Lemma 11. *There exists a constant $\theta > 1$ satisfying $F_{min}(s,i) \geq \theta\bar{F}_{\mathbf{c}}(s)$, where $3 \leq i \leq 5$.*

Proof. Let us start with the case $i = 5$. We need to prove that there exists $\theta_5 > 1$, such that $F_{min}(s,5) \geq \theta_5\bar{F}_{\mathbf{c}}(s)$. Let $V_5(s,\mathbf{c})$ be a Voronoi cell of $\mathbf{c}$ with five neighbours and with area s realizing the minimum HM CVT energy $F_{min}(s,5)$. By Lemma 10, we need only to show that $|V_5(s,\mathbf{c}) \setminus U(s,\mathbf{c})|$ (i.e., the area of the boolean difference of $V_5(s,\mathbf{c})$ and $U(s,\mathbf{c})$) is αs, where α is a positive constant.

We shall prove by contradiction. Assume that $\nexists\, \alpha > 0$ such that $|V_5(s,\mathbf{c}) \setminus U(s,\mathbf{c})| \geq \alpha s$.

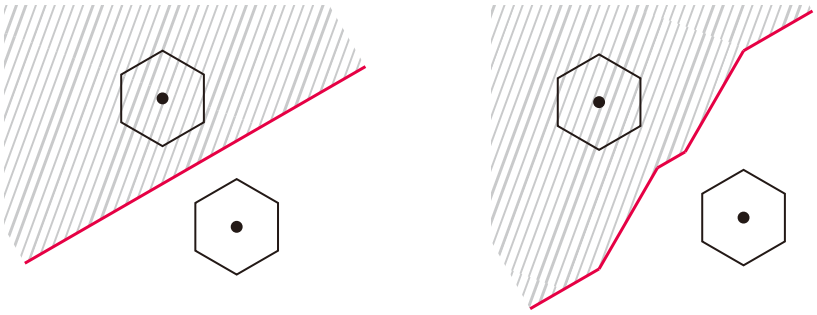

Figure B.8: Two types of bisectors (in red) of neighbouring seeds.

We first note that the boundary of $V_5(s,\mathbf{c})$ comprises five Voronoi edges, each being a bisector of $\mathbf{c}$ and one of its five neighbouring seeds. A bisector between two seeds is either a line segment or a polyline composing of at most five line segments, as illustrated in the left and right images in Figure B.8, respectively, with the obtuse angle between two adjacent line segments being $\frac{5\pi}{6}$. A bisector partitions the two-dimensional planar domain into two regions, one of which contains the seed $\mathbf{c}$. The intersection of five such regions defines $V_5(s,\mathbf{c})$.

Given any point $\mathbf{p}$ on the boundary of $U(s,\mathbf{c})$, if the distance from $\mathbf{p}$ to the boundary of $V_5(s,\mathbf{c})$ is ϵ, where ϵ is a positive constant, then we may construct a disk of radius ϵ centered at $\mathbf{p}$. The disk is partitioned by the boundary of $U(s,\mathbf{c})$ into two regions, one of which is contained either in $V_5(s,\mathbf{c}) \setminus U(s,\mathbf{c})$ or in

$U(s,\mathbf{c}) \setminus V_5(s,\mathbf{c})$, and is with area no less than $\frac{\pi\epsilon^2}{3}$. Since $|V_5(s,\mathbf{c}) \setminus U(s,\mathbf{c})| = |U(s,\mathbf{c}) \setminus V_5(s,\mathbf{c})|$, we have $|V_5(s,\mathbf{c}) \setminus U(s,\mathbf{c})| \geq \alpha s$, where $\alpha = \frac{\pi\epsilon^2}{3s}$. Due to the assumption that $\nexists\, \alpha > 0$, $|V_5(s,\mathbf{c}) \setminus U(s,\mathbf{c})| \geq \alpha s$, we conclude that the distance from any point $\mathbf{p}$ on the boundary of $U(s,\mathbf{c})$ to the boundary of $V_5(s,\mathbf{c})$ is less than ϵ for any $\epsilon > 0$, and hence $\mathbf{p}$ must lie on the boundary of $V_5(s,\mathbf{c})$. In other words, the boundary of $V_5(s,\mathbf{c})$ contains the boundary of $U(s,\mathbf{c})$.

Now, the boundary of $U(s,\mathbf{c})$ is a polyline of six line segments in which the angle between any two adjacent segments is $\frac{2\pi}{3}$. However, there is at most five angles which are equal to $\frac{2\pi}{3}$ on the boundary of $V_5(s,\mathbf{c})$. This yields a contradiction.

Following similar arguments, we may find $\theta_4 > 1$ and $\theta_3 > 1$, for the cases $i = 4$ and $i = 3$, respectively. Finally, we choose $\theta = \min\{\theta_3, \theta_4, \theta_5\}$, and this completes the proof. □

Lemma 12.

$$m - m_6 = o(m), \quad as \;\; m \to \infty.$$

Proof. Lemma 9 shows that the average number of neighbours of all Voronoi cells is 6. So we need only to show that the number of Voronoi cells with less than six neighbours is $o(m)$. We will show it by contradiction. Assume $m_3 + m_4 + m_5 = \alpha m$, where α is a positive constant. Then, we have

$$\begin{aligned} F_H(\mathbf{X}_m) &= \sum_{i=3}^{k}\sum_{j=1}^{m_i} F_{D_{ij}}(\mathbf{X}_m) \\ &\geq \sum_{i=3}^{5}\sum_{j=1}^{m_i} \theta \bar{F}_{\mathbf{c}}(|D_{ij}|) + \sum_{i=6}^{k}\sum_{j=1}^{m_i} \bar{F}_{\mathbf{c}}(|D_{ij}|), \end{aligned}$$

where θ is the same quantity as in Lemma 11. Now, we have two cases:

Case 1:
$\frac{\sum_{i=3}^{5}\sum_{j=1}^{m_i}|D_{ij}|}{m_3+m_4+m_5} = o(\frac{1}{m})$. The average area of all Voronoi cells with 3, 4 and 5 neighbours is $o(\frac{1}{m})$.
Hence, $\sum_{i=3}^{5}\sum_{j=1}^{m_i}|D_{ij}| = o(\alpha) = o(1)$.

Then, we have $\sum_{i=6}^{k}\sum_{j=1}^{m_i}|D_{ij}| \sim 1$, and $\frac{\sum_{i=6}^{k}\sum_{j=1}^{m_i}|D_{ij}|}{m_6+\ldots+m_k} \sim \frac{1}{m_6+\ldots+m_k} = \frac{1}{(1-\alpha)m}$. Therefore,

$$\begin{aligned}
&\sum_{i=3}^{5}\sum_{j=1}^{m_i}\theta\bar{F}_{\mathbf{c}}(|D_{ij}|) + \sum_{i=6}^{k}\sum_{j=1}^{m_i}\bar{F}_{\mathbf{c}}(|D_{ij}|) \\
&\quad\geq \sum_{i=3}^{5}\sum_{j=1}^{m_i}\theta\bar{F}_{\mathbf{c}}(|D_{ij}|) + (m_6+\ldots+m_k)\bar{F}_{\mathbf{c}}(\frac{1}{(1-\alpha)m}) \\
&\quad= \sum_{i=3}^{5}\sum_{j=1}^{m_i}\theta\bar{F}_{\mathbf{c}}(|D_{ij}|) + (1-\alpha)m\bar{F}_{\mathbf{c}}(\frac{1}{(1-\alpha)m}) \\
&\quad= \sum_{i=3}^{5}\sum_{j=1}^{m_i}\theta\bar{F}_{\mathbf{c}}(|D_{ij}|) + \frac{1}{1-\alpha}m\bar{F}_{\mathbf{c}}(\frac{1}{m}) \\
&\quad> \sum_{i=3}^{5}\sum_{j=1}^{m_i}\theta\bar{F}_{\mathbf{c}}(|D_{ij}|) + m\bar{F}_{\mathbf{c}}(\frac{1}{m})
\end{aligned}$$

and hence a contradiction.

Case 2: $\frac{\sum_{i=3}^{5}\sum_{j=1}^{m_i}|D_{ij}|}{m_3+m_4+m_5} = \frac{\beta}{m}$, for some non-zero constant β. The average area of all Voronoi cells with 3, 4 and 5 neighbours is $\frac{\beta}{m}$. Therefore,

$$\begin{aligned}
&\sum_{i=3}^{5}\sum_{j=1}^{m_i}\theta\bar{F}_{\mathbf{c}}(|D_{ij}|) + \sum_{i=6}^{k}\sum_{j=1}^{m_i}\bar{F}_{\mathbf{c}}(|D_{ij}|) \\
&\quad= \sum_{i=3}^{5}\sum_{j=1}^{m_i}(\theta-1)\bar{F}_{\mathbf{c}}(|D_{ij}|) + \sum_{i=3}^{5}\sum_{j=1}^{m_i}\bar{F}_{\mathbf{c}}(|D_{ij}|) + \sum_{i=6}^{k}\sum_{j=1}^{m_i}\bar{F}_{\mathbf{c}}(|D_{ij}|) \\
&\quad\geq (\theta-1)\alpha m\bar{F}_{\mathbf{c}}(\frac{\beta}{m}) + m\bar{F}_{\mathbf{c}}(\frac{1}{m}) \\
&\quad= (\theta-1)\alpha\beta^2 m\bar{F}_{\mathbf{c}}(\frac{1}{m}) + m\bar{F}_{\mathbf{c}}(\frac{1}{m})
\end{aligned}$$

and hence a contradiction.

Each case yields a contradiction under the assumption given in Theorem 1. □

Remark 1. *The idea in the proof is not applicable if the Euclidean metric is used in place of the HM metric. The difference between the HM metric and the Euclidean metric is that under the HM metric, a Voronoi cell whose area is s and whose number of neighbours is not six has larger energy than $\bar{F}_{\mathbf{c}}(s)$. However, it is not true under the Euclidean metric in which given fixed area s, a Voronoi cell with 7 neighbours may have smaller energy than a regular hexagonal Voronoi cell.*

Lemma 13. *Let m_{6r} denote the number of Voronoi cells with six neighbours whose area differs from $\frac{|\Omega|}{m}$ by $o(\frac{|\Omega|}{m})$, then*

$$m - m_{6r} = o(m), \quad as \quad m \to \infty.$$

Proof. We shall prove by contradiction. We call a Voronoi cell *bad* if the difference between its area and $\frac{|\Omega|}{m}$ is not $o(\frac{|\Omega|}{m})$; we have m_{bad} bad Voronoi cells and $m_{bad} = m - m_{6r} \geq \beta m$, where β is a positive constant. Recall that D_{6j}, $j = 1, \ldots, m_6$, are all the Voronoi cells with 6 neighbours. Without loss of generality, we assume that D_{6k}, $k = 1, \ldots, m_{bad}$, are the bad Voronoi cells and the difference between the area of each of these cells and $\frac{|\Omega|}{m}$ is at least $\alpha\frac{|\Omega|}{m}$, where α is a positive constant.

Since $m - m_6 = o(m)$, and $\max_{\mathbf{p}\in\mathbf{X}_m}\{diam\big(VC(\mathbf{p})\bigcap int(\Omega)\big)\} \sim 0$ as $m \to \infty$, we conclude that

$$\frac{\sum_{j=1}^{m_6}|D_{6j}|}{m_6} \sim \frac{|\Omega|}{m}.$$

From

$$\frac{\sum_{j=m_{bad}+1}^{m_6}|D_{6j}|}{m_6 - m_{bad}} \sim \frac{|\Omega|}{m},$$

we have

$$\frac{\sum_{j=1}^{m_{bad}}|D_{6j}|}{m_{bad}} \sim \frac{|\Omega|}{m}.$$

Then, we have

$$\begin{aligned}
F_H(\mathbf{X}_m) &= \sum_{i=3}^{k}\sum_{j=1}^{m_i} F_{D_{ij}}(\mathbf{X}_m) \\
&\geq \sum_{i\neq 6}\sum_{j=1}^{m_i}\bar{F}_{\mathbf{c}}(|D_{ij}|) + \sum_{j=1}^{m_6}\bar{F}_{\mathbf{c}}(|D_{6j}|) \\
&= \sum_{i\neq 6}\sum_{j=1}^{m_i}\bar{F}_{\mathbf{c}}(|D_{ij}|) + \sum_{j=1}^{m_{bad}}\bar{F}_{\mathbf{c}}(|D_{6j}|) + \sum_{j=m_{bad}+1}^{m_6}\bar{F}_{\mathbf{c}}(|D_{6j}|) \\
&\geq \sum_{i\neq 6} m_i\bar{F}_{\mathbf{c}}(\frac{\sum_{i\neq 6}\sum_{j=1}^{m_i}|D_{ij}|}{\sum_{i\neq 6} m_i}) \\
&\quad + (1+\alpha^2)m_{bad}\bar{F}_{\mathbf{c}}(\frac{\sum_{j=1}^{m_{bad}}|D_{6j}|}{m_{bad}}) \\
&\quad + (m_6 - m_{bad})\bar{F}_{\mathbf{c}}(\frac{\sum_{j=m_{bad}+1}^{m_6}|D_{6j}|}{m_6 - m_{bad}}) \\
&\geq m\bar{F}_{\mathbf{c}}(\frac{|\Omega|}{m}) + \alpha^2\beta m\bar{F}_{\mathbf{c}}(\frac{|\Omega|}{m})
\end{aligned}$$

which contradicts to the assumption given in Theorem 1. □

Lemma 14. *Let $\tilde{\Omega}_{6rg}$ be the set of all Voronoi cells have 6 neighbours; further, for any Voronoi cell $\Omega_i \in \tilde{\Omega}_{6rg}$, we have the area of the boolean difference of Ω_i and $U(|\Omega_i|, \mathbf{x}_i)$ be $o(\frac{|\Omega|}{m})$. Let $m_{6rg} = |\tilde{\Omega}_{6rg}|$. Then,*

$$m - m_{6rg} = o(m), \ \ as \ \ m \to \infty.$$

Proof. We shall prove by contradiction. We call a Voronoi cell Ω_i *bad* if the area of the boolean difference of Ω_i and $U(|\Omega_i|, \mathbf{x}_i)$ is not $o(\frac{|\Omega|}{m})$. Let there be m_{bad} Voronoi cells and we have $m_{bad} = m - m_{6rg} \geq \beta m$, where β is a positive constant. Since the area of the boolean difference of a bad Voronoi cell Ω_i of $\mathbf{x}_i$ and $U(|\Omega_i|, \mathbf{x}_i)$ is at least $\alpha(|\Omega_i|)$, where α is a positive constant, we can find a constant $\gamma > 1$, such that $F_{\mathbf{x}_i}(\Omega_i) \geq \gamma \bar{F}_{\mathbf{c}}(|\Omega_i|)$. Therefore, we have $F_H(\mathbf{X}_m) \geq m\bar{F}_{\mathbf{c}}(\frac{|\Omega|}{m}) + (\gamma - 1)\beta m \bar{F}_{\mathbf{c}}(\frac{|\Omega|}{m})$, yielding the contradiction. □

Proof of Theorem 1: From Lemma 14, we can see that $\mathbf{X}_m$ is asymptotically a regular hexagonal pattern, in which the hexagons are with the same orientation as H. A simple calculation also shows that the edge length of the regular hexagon is $(\frac{2|\Omega|}{3\sqrt{3}m})^{1/2}$. Theorem 1 is thus proved. □

Appendix C. Proof of Theorem 2

We assume the Riemannian metric defined on the domain Ω is the same everywhere.

Definition 1 (Centrosymmetric Seed)**.** *A seed s is called a Centrosymmetric Seed (CS) if its neighbouring seeds (i.e., those seeds sharing at least one Voronoi edge with s) in the Voronoi diagram is centrosymmetric with respect to s.*

Definition 2 (Centrosymmetric Voronoi Cell)**.** *A Voronoi cell is called a Centrosymmetric Voronoi Cell (CVC) if it is centrosymmetric with respect to the seed of the cell.*

Definition 3 (Centrosymmetric Pattern)**.** *Given a set of seeds $\mathbf{Y}$, if each Voronoi cell of $\mathbf{Y}$ is a CVC, then $\mathbf{Y}$ form a Centrosymmetric Pattern (CP).*

Lemma 15. *If a seed is a CS, its Voronoi cell is a CVC.*

Proof: The proof is straightforward and is omitted here. □

Theorem 2. *Given a set of seeds $\mathbf{Y}$, if $\mathbf{Y}$ consists of only centrosymmetric seeds, the partial derivative of $F_H(\mathbf{Y})$ with respect to each seed in $\mathbf{Y}$ is zero.*

Proof: Since each seed in $\mathbf{Y}$ is a CS, its Voronoi cell is a CVC. A simple calculation shows that the partial derivative with respect to such a seed is zero. □